Materials Horizons

ROYAL SOCIETY OF CHEMISTRY

COMMUNICATION

View Article Online
View Journal | View Issue

Cite this: *Mater. Horiz.*, 2021, 8, 1518

Received 27th December 2020,
Accepted 1st March 2021

DOI: 10.1039/d0mh02051f

rsc.li/materials-horizons

Metal- and halide-free, solid-state polymeric water vapor sorbents for efficient water-sorption-driven cooling and atmospheric water harvesting†

Mengchun Wu,[a] Renyuan Li,[a] Yusuf Shi,[a] Mustafa Altunkaya,[b] Sara Aleid,[a] Chenlin Zhang,[a] Wenbin Wang[a] and Peng Wang *[ac]

Metal- and halide-free, solid-state water vapor sorbents are highly desirable for water-sorption-based applications, because most of the solid sorbents suffer from low water sorption capacity caused by their rigid porosity, while the liquid sorbents are limited by their fluidity and strong corrosivity, which is caused by the halide ions. Herein, we report a novel type of highly efficient and benign polymeric sorbent, which contains no metal or halide, and has an expandable solid state when wet. A group of sorbents are synthesized by polymerizing and cross-linking the metal-free quaternary ammonium monomers followed by an ion-exchange process to replace chloride anions with benign-anions, including acetate, oxalate, and citrate. They show significantly reduced corrosivity and improved water sorption capacity. Importantly, the water sorption capacity of the acetate paired hydrogel is among the best of the literature reported hygroscopic polymers in their pure form, even though the hydrogel is crosslinked. The hydrogel-based sorbents are further used for water-sorption-driven cooling and atmospheric water harvesting applications, which show improved coefficient of performance (COP) and high freshwater production rate, respectively. The results of this work would inspire more research interest in developing better water sorbents and potentially broaden the application horizon of water-sorption-based processes towards the water-energy nexus.

New concepts

Water vapor sorbents are the key components in various emerging water-sorption-based applications, such as sorption-based cooling/heating technologies, atmospheric freshwater harvesting, vapor-sorption-based desalination, and air humidity regulation. Most of these applications can be driven by solar energy alone, making them very promising in establishing a greener and more sustainable world. However, most of the solid sorbents suffer from a low water sorption capacity, while the liquid sorbents are limited by their fluidity and strong corrosivity. Here, for the first time, we report a novel type of metal- and halide-free, solid-state polymeric water vapor sorbents with improved water vapor sorption capacity, reduced corrosivity, and solid state when wet. To achieve this, we demonstrate a new concept to fabricate polymeric sorbents by polymerizing and crosslinking the metal-free quaternary ammonium monomers followed by an ion-exchange process to replace halide anions with benign-anions. The as-developed polymeric sorbents exhibit (1) high water vapor sorption capacity thanks to the deliquescent nature of quaternary ammonium cations and benign-anions; (2) reduced corrosivity due to the halide-free nature of benign-anions; and (3) solid state when wet due to the crosslinked structure. As such, the halide-free sorbents show improved coefficient of performance (COP) and high freshwater production rate in water-sorption-driven cooling and atmospheric water harvesting applications.

1. Introduction

Due to the ever-worsening global warming, increasing global population, and steady improvement of life standards, adequate clean water and stable supply of clean energy with low carbon footprint are two key challenges for global sustainable development.[1–8] On the other hand, there is a vast amount of water constantly preserved in the Earth's atmosphere, generically known as atmospheric water, which is equivalent to six times all the water in all the rivers on Earth.[6,9] The capture-release of water vapor has underpinned a number of emerging designs significant to the water-energy nexus, such as sorption-driven heat transformation for cooling and heating,[10–14] atmospheric water harvesting (AWH),[15–28] vapor-sorption-based desalination,[14,29] and air humidity regulation.[30,31] In particular, sorption-driven cooling and AWH are gaining a lot of interest nowadays in both academia and industry as they aim at reducing electricity consumption, obsoleting the conventional harmful coolants (*e.g.*, chlorodifluoromethane, 1,1,1,2-tetrafluoroethane),[32] and producing

[a] *Water Desalination and Reuse Center, Division of Biological and Environmental Science and Engineering, King Abdullah University of Science and Technology, Thuwal 23955-6900, Saudi Arabia. E-mail: peng.wang@kaust.edu.sa, peng1.wang@polyu.edu.hk*

[b] *Analytical Chemistry Core Laboratories (ACL), King Abdullah University of Science and Technology, Thuwal 23955-6900, Saudi Arabia*

[c] *Department of Civil and Environmental Engineering, The Hong Kong Polytechnic University, Hung Hom, Kowloon, Hong Kong, China*

† Electronic supplementary information (ESI) available. See DOI: 10.1039/d0mh02051f

freshwater from an unconventional source (the atmosphere). In all of these applications, the water vapor sorbent is the most critical component. The performance of these systems can be directly determined by the water exchange capacity of the sorbents during the water vapor sorption and desorption stages and the energy required for the regeneration of the water vapor sorbents.

For most inorganic porous solid sorbents, such as silica gel and zeolite, their water sorption capacities are limited by their small pore volume.[14] Very recently, several specially designed MOF-type materials have been reported to possess higher water sorption capacity and thus give enhanced performance in these applications.[10] However, the use of special organic ligands and toxic metals in making these materials increases the capital, maintenance and disposal costs. Liquid sorbents, like the aqueous solution of hygroscopic inorganic salts (*e.g.*, LiCl, $CaCl_2$), possess much higher water sorption capacity and lower regeneration energy demand, making them have high energy efficiency in these applications.[6,19] However, the liquid form, unavoidable salt creeping phenomenon and highly corrosive halide ions bring numerous practical difficulties in handling, sealing, and anticorrosive requirements. Integrating hygroscopic inorganic salts with hydrogels or porous matrices can partially solve the liquidity problem,[9,13–18,33–35] such as incorporating $CaCl_2$ into polyacrylamide (PAM) hydrogel or poly(*N*-isopropylacrylamide) (PNIPAM)–MOF mixed matrix hydrogel,[9,15,18] integrating $CaCl_2$ and LiCl binary salts into sodium alginate hydrogel,[34] and integrating LiBr into PAM hydrogel,[35] but the salt creeping and corrosive halide still remain great challenges. In addition, some of their major elements, especially lithium, have limited and dwindling reserved stock on Earth.[36,37]

Recently, organic materials have been investigated as alternative water vapor sorbents because of their low-cost, less toxicity, and the wide pool of potential candidates. Hygroscopic polymers,[20–22,38–46] like poly(acrylic acid) sodium salt (PAAS),[21,38] chloride-doped polypyrrole (PPy-Cl),[20,43,44] sodium alginate (Alg),[41] poly(diallyldimethylammonium chloride) (PDDA),[45] *etc.*, as well as glycerin,[23] and ionic liquid,[24,29,36,46] are mostly reported. However, much like the inorganic salt-based sorbents, the non-crosslinked hygroscopic polymers, glycerin, and ionic liquid, all work in liquid form. Besides, there is a dilemma in these reported materials: the halide-free polymers possess significantly lower water sorption capacities while the halide-containing polymers suffer from strong corrosivity. Therefore, the development of metal- and halide-free, solid-state water vapor sorbents with high water sorption capacity are highly sought after.

In this work, we rationally chose metal-free quaternary ammonium monomer, *i.e.* [2-(acryloyloxy)ethyl]trimethylammonium chloride solution (AETA-Cl), as the hygroscopic component, and synthesized a novel type of solid-state water vapor sorbent through polymerization, crosslinking, and ion-exchange. The synthesis of polymers and their crosslinking are facile, and the crosslinked polymers form elastic hydrogels that maintain the solid-state at all times. The counter anion (*i.e.*, chloride) of the hydrogels was easily exchanged with benign-anions (*e.g.*, acetate, oxalate, and citrate). After the ion-exchange, the as-developed hydrogel sorbents have the advantages of solid-state after water vapor sorption, improved water vapor sorption capacities, and reduced metal corrosivity. The hydrogel paired with acetate (PAETA–Ac) showed an improved water uptake of ~ 0.31 g g^{-1} at a low relative humidity (RH) of 30%, and an increased water uptake of ~ 0.87 g g^{-1} at RH of 80%, which is the highest number for any reported polymeric water sorbents in their pure form without inorganic salt and any other additives. It is even higher than those non-crosslinked polymers like PPy-Cl (~ 0.18 g g^{-1}),[20] PAAS (~ 0.58 g g^{-1}),[38] and PDDA (~ 0.80 g g^{-1}).[45] For a typical air-conditioning application, PAETA–Ac produced a coefficient of performance (COP) of 0.75 for cooling with a temperature lift of 20 °C at a low sorbent regeneration temperature (~ 70 °C). The low regeneration temperature of the sorbent enables the use of low-grade industrial waste heat or heat generated from solar energy by simple solar-thermal conversion in both cooling and AWH applications. The outdoor field AWH experimental results showed that PAETA–Ac can produce ~ 0.53 g g^{-1} freshwater from one cycle of water vapor sorption and desorption. All of these results show that the metal- and halide-free solid-state polymeric vapor sorbents first reported in this work have the potential to make a solid contribution to the global water-energy nexus.

2. Results and discussion

Fabrication of PAETA–X

Fig. 1a presents the synthetic procedure of the polycationic hydrogels paired with different counter anions. The PAETA–Cl hydrogel was first synthesized *via* polymerization of a quaternary ammonium-based monomer, *i.e.*, AETA-Cl, with *N*,*N*′-methylenebisacrylamide (BIS) as the crosslinking agent. After the polymerization and crosslinking, liquid AETA-Cl monomer solution (Fig. S1a, ESI†) was transformed into a solid hydrogel (Fig. S1b, ESI†). The hydrogel was flexible and could be cut into small pieces without structural collapse (Fig. S1c, ESI†). Subsequently, an ion-exchange process was conducted to exchange the Cl^- anion with acetate (Ac^-), oxalate (Ox^{2-}), or citrate (Cit^{3-}) counter anions, respectively. The as-prepared polycationic hydrogels are denoted as PAETA–*X*, where *X* represents the counter anion of Cl^-, Ac^-, Ox^{2-}, and Cit^{3-}, respectively. Since quaternary ammonium cations and carboxylate anions are well known as the deliquescent components that can attract water molecules,[21,24,39,45] an AETA-based cation and Ac^-, Ox^{2-}, and Cit^{3-} are rationally chosen for the fabrication of Cl-free water vapor sorbents. The Cl-free PAETA–X hydrogels can sorb water vapor from ambient air and desorb the water vapor under a low temperature or sunlight irradiation (Fig. 1b), which can be used for energy-efficient water-sorption-driven cooling and AWH applications.

Attenuated total reflection-Fourier transform infrared spectroscopy (ATR-FTIR) and energy-dispersive X-ray spectroscopy (EDS) were used to analyze the chemical composition of the synthesized hydrogels. Fig. 2a shows the ATR-FTIR spectra of PAETA–X hydrogels, where the characteristic peaks at ~ 1726, ~ 1160, ~ 1479, and ~ 950 cm^{-1} are due to the C=O and C–O–C stretching of esters, $-CH_3$ bending vibration and stretching vibration of quaternary ammonium $[R–N(CH_3)_3]^+$, respectively.[47] These characteristic peaks persist in the FTIR spectra before and after

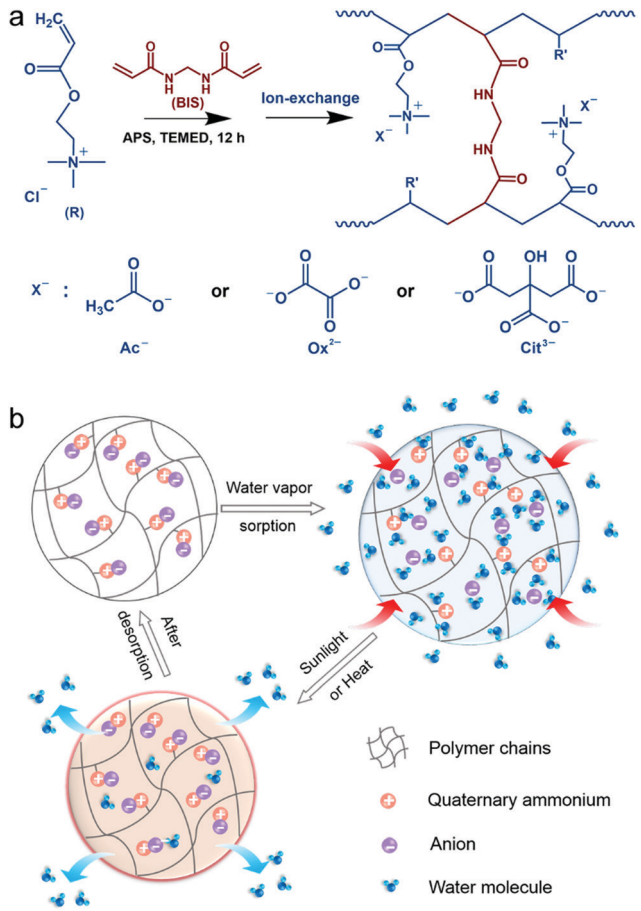

Fig. 1 (a) Schematic illustration of the synthetic procedure of PAETA–X hydrogels paired with Cl^-, Ac^-, Ox^{2-}, and Cit^{3-} counter anions. (b) Schematic illustration of PAETA–X hydrogel with reversible water vapor sorption and desorption properties.

the ion-exchange, indicating that the ion-exchange step does not affect the chemical composition of the polycationic matrices (*i.e.*, PAETA). After replacing Cl^- with Ac^-, Ox^{2-}, and Cit^{3-}, the characteristic IR bands attributed to Ac^-, Ox^{2-}, and Cit^{3-} were observed in the FTIR spectra of the resultant hydrogels. Specifically, in the FTIR spectrum of PAETA–Ac hydrogel, the bands that appeared at ~1567 and ~1391 cm^{-1} correspond to asymmetric and symmetric C–O stretching vibrations from carboxylate ions (COO^-) of acetate anions.[24] For PAETA–Ox hydrogel, the characteristic bands at ~1557 and ~1296 cm^{-1} are from asymmetric and symmetric C–O stretching modes of $C_2O_4^{2-}$.[48] For PAETA–Cit hydrogel, the characteristic bands at ~1570 and ~1376 cm^{-1} are associated with asymmetric and symmetric COO^- stretching of citrate anions, and the band centered at ~1376 cm^{-1} shows the presence of two shoulders (Fig. S2, ESI†), which is attributed to the non-equivalent environments of the three carboxylate groups.[49] Moreover, the high-intensity EDS signals of Cl^- in PAETA–Cl completely disappeared in PAETA–Ac, PAETA–Ox, and PAETA–Cit hydrogels (Fig. 2b). These results all indicate the successful synthesis and solid form stability of PAETA–X hydrogels.

The thermal stabilities of PAETA–X hydrogels were determined by thermogravimetric analysis (TGA), and the resultant TGA curves are presented in Fig. 2c. As can be seen, the first degradation of PAETA–X can be assigned to the decomposition of pendant quaternary ammonium groups. The extrapolated onset temperature (T_{onset}) of PAETA–X hydrogels can be used to denote the temperature at which a weight loss begins and was in the order of PAETA–Cl (236 °C) > PAETA–Cit (174 °C) > PAETA–Ox (173 °C) > PAETA–Ac (163 °C). After the ion-exchange, the T_{onset} of the carboxylate-containing PAETA–X hydrogels was lower than that of PAETA–Cl, which was presumably because the nucleophilicity of carboxylate-containing anions is greater than that of chloride anions. Thus the pyrolysis of these carboxylate-containing PAETA–X hydrogels *via* an S_N2 reaction might occur at lower temperatures.[50]

The glass transition temperatures (T_g) of PAETA–X hydrogels were investigated *via* differential scanning calorimetry (DSC). As shown in Fig. 2d (left), in the dry state, the T_g of PAETA–X hydrogels decreased from ~92.0 °C when "*X*" is Cl^- to ~91.9, ~81.2, or ~66.6 °C when "*X*" is Cit^{3-}, Ox^{2-}, and Ac^-, respectively. Compared with PAETA–Cl, PAETA–Ac shows a lower T_g which is caused by the increased size and reduced charge density of the counter anions.[51] Compared with PAETA–Ac, the higher T_g values of PAETA–Ox and PAETA–Cit are due to the existence of ionic crosslinking between the di-/tri-carboxylate ligands and polymer side chains. In the dry state, the T_g values of all PAETA–X hydrogels are higher than room temperature, indicating their glassy state at room temperature.

The T_g values of PAETA–X hydrogels were also analyzed in the wet state after a 6 h water sorption process under ambient conditions. In the wet state (Fig. 2d, right), the T_g values of all PAETA–X hydrogels were reduced to below 0 °C, indicating that PAETA–X hydrogels have a rubbery state when wet. This is because water molecules penetrate into the hydrophilic polymer matrix and bind to the polar groups of the polymer chains, which weakens the interactions among the polymer chains, consequently leading to the plasticization of PAETA–X hydrogels and an increase of their molecular mobility and free volume.[52]

Water vapor sorption properties

The water vapor sorption capacities (*W*) of PAETA–X hydrogels were firstly investigated under dynamic RH conditions at 25 °C. As shown in Fig. 3a, PAETA–X hydrogels immediately began to sorb water once the RH started to rise from ~0%, indicating that PAETA–X hydrogels can be used to sorb water vapor at low RH (*e.g.*, ≲30%). For instance, under the conditions of 25 °C with 30% RH, PAETA–X hydrogel sorbed ~0.19, 0.31, 0.25, and 0.21 g of water (g g^{-1}) when the anion was Cl^-, Ac^-, Ox^{2-}, and Cit^{3-}, respectively. The water sorption capacity was increased with increasing RH. At RH of 80%, the water sorption capacity of the PAETA–X hydrogel was increased to ~0.62, 0.87, 0.74, and 0.66 g g^{-1}, with the anion of Cl^-, Ac^-, Ox^{2-}, and Cit^{3-}, respectively.

The water vapor sorption capacity of PAETA–X hydrogel with different anions was in the order of Ac^- > Ox^{2-} > Cit^{3-} > Cl^- under all RH conditions, which was presumably because after the ion-exchange process, the mobility of the polymer chains is increased and the hydrogen-bond basicity of the anions is

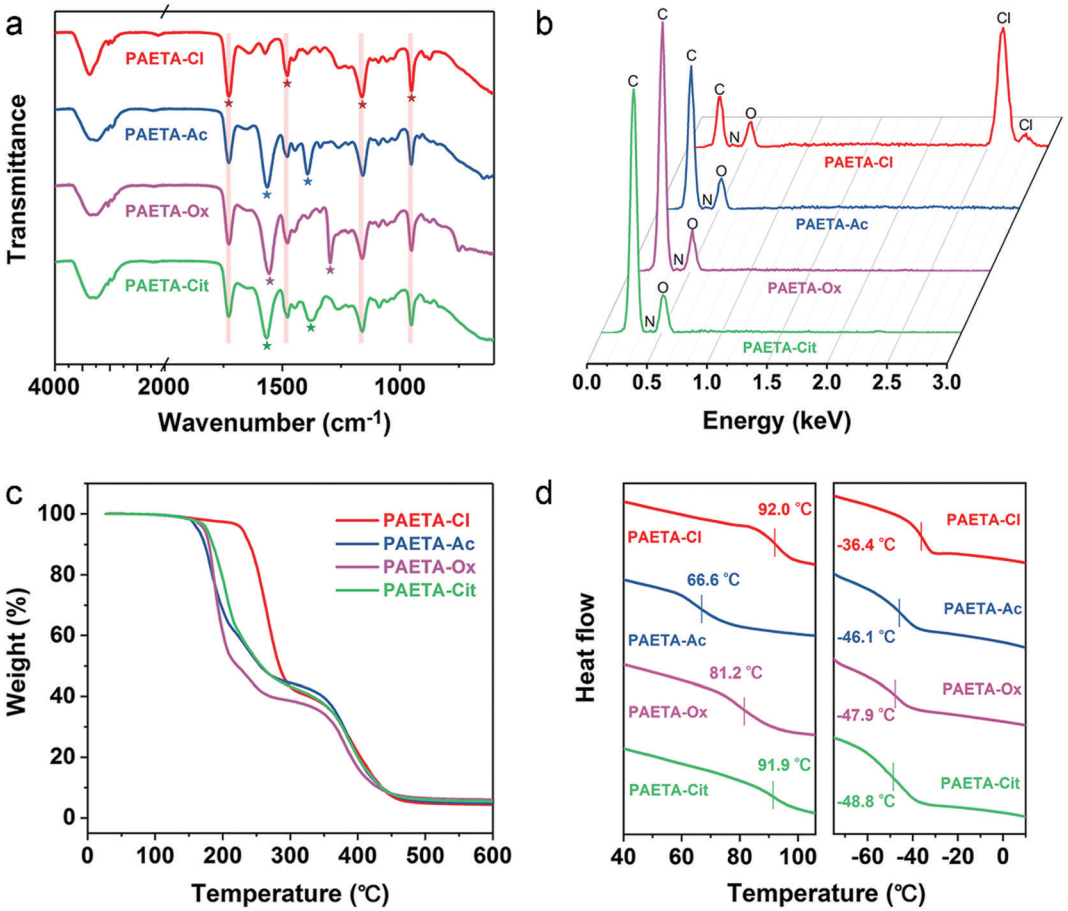

Fig. 2 (a) ATR-FTIR spectra, (b) EDS spectra, (c) TGA curves, and (d) DSC curves (left: dry, right: wet) of PAETA–Cl, PAETA–Ac, PAETA–Ox, and PAETA–Cit hydrogels.

increased by introducing carboxylate ions.[46,53] Among all, PAETA–Ac shows the highest water sorption capacity ($\sim$0.87 g g^{-1} at 25 °C, 80% RH), higher than other metal- and halide-free polymeric sorbents reported in the literature under the same conditions, such as an epoxy-functionalized porous organic polymer (ep-POP, $<$0.4 g g^{-1}), and a pseudoprotein-based fully organic polymeric desiccant ($<$0.09 g g^{-1}).[22,40] Importantly, the water vapor sorption capacity of PAETA–Ac hydrogel is among the best in the reported hygroscopic polymers in their pure form and traditional desiccants (*e.g.*, silica gel and zeolite), even though the PAETA–Ac hydrogel was crosslinked in this case (Fig. S3, ESI†). PAETA–X hydrogels show higher water vapor sorption capacity due to the existence of two types of highly hygroscopic groups, *i.e.*, the quaternary ammonium group and carboxylate group.[21,24,39,45] Compared with other typical sorbents, although PAETA–X hydrogel shows lower water sorption capacity ($\sim$0.87 g g^{-1} at 80% RH) than some MOFs ($\sim$0.95 g g^{-1}),[54] hygroscopic salts (*e.g.*, LiCl, $CaCl_2$, $>$1.5 g g^{-1}),[15,19,34] and ionic liquids ($>$1.0 g g^{-1}),[24] its advantages of halide free, facile fabrication, and solid state make PAETA–X hydrogel an attractive sorbent.

The water vapor sorption and desorption isotherms of PAETA–X hydrogels at 25 °C and 50 °C were measured (Fig. 3b), based on which the enthalpy of sorption ($\Delta_s H$) for water was calculated (Supplementary Note S1 and Eqn S1 in the ESI†). As shown in Fig. 3c, the $\Delta_s H$ values were relatively high when the water uptake was low, due to the fact that the initial sorbed water molecules have relatively strong interactions with the polymer hydrophilic groups.[24] As the water uptake increased, the $\Delta_s H$ values were gradually reduced to constant values of about -45 kJ mol^{-1}, -46 kJ mol^{-1}, -46 kJ mol^{-1}, and -46 kJ mol^{-1} for PAETA–Cl, PAETA–Ac, PAETA–Ox, and PAETA–Cit, respectively. The constant $\Delta_s H$ values are close to the enthalpy of water evaporation ($\sim$44 kJ mol^{-1} at 30 °C), indicating that hydrogen bond interactions among water molecules play a dominant role therein.[13,24]

The water vapor sorption kinetics were evaluated by conducting a static RH test at 25 °C in a nitrogen flow with RH of 60%. The results show that PAETA–X hydrogels possess a fast vapor sorption kinetics, with the sorption equilibrium being achieved within 3 hours (Fig. 3d and e). In comparison, $CaCl_2$ liquid sorbent,[19] glycerin-based organogel sorbent,[23] IL sorbent,[24] $CaCl_2$/PAM sorbent,[15] LiCl/$CaCl_2$/alginate sorbent,[34] *etc.*, all require more than 12 hours to reach the sorption equilibrium. In the desorption process at 70 °C, $\sim$90% of the sorbed water was released from PAETA–X hydrogels within 0.5 hour, while the

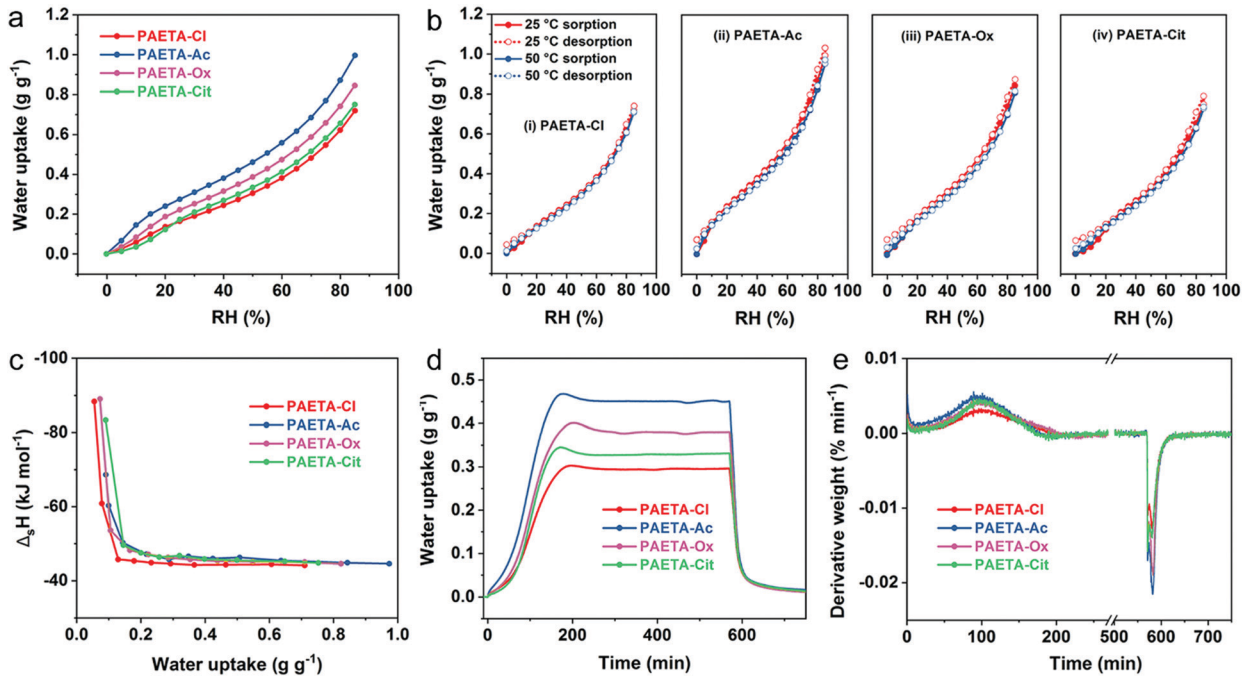

Fig. 3 (a) Water vapor sorption isotherms at 25 °C, (b) water vapor sorption and desorption isotherms at 25 °C and 50 °C, (c) $\Delta_s H$ as a function of water vapor uptake, (d) static water sorption–desorption curves, and (e) 1st derivative curves of static water sorption–desorption for PAETA–X hydrogels.

remaining ~10% of water, due to its relatively strong interactions with the hydrophilic groups of the polymer, was released within the next 2.5 hours. The high-water sorption capacity, fast sorption and desorption kinetics, and low regeneration temperature of PAETA–X are conducive to enhanced cooling energy efficiency and atmosphere water production, which are to be presented and discussed later.

Since PAETA–X hydrogels all have the same quaternary ammonium cation group, the different anions are considered as the major factors affecting the water sorption capacity. First, Cl^- and Ac^- were compared because both of them are single-charged. The binding energy (ΔE) and coordination number of Cl^- and Ac^- with water molecules were calculated.[55] As can be seen in Fig. S4 (ESI†), ΔE of Ac^- (-407.50 ± 23.97 kJ mol^{-1}) is lower than that of Cl^- (-290.51 ± 19.27 kJ mol^{-1}), indicating that Ac^- has stronger interactions with water molecules, has higher water affinity and can attract water molecules more easily than Cl^-. On the other hand, the coordination number of Ac^- (~8.6) is larger than that of Cl^- (~7.8), indicating that Ac^- can bind with more water molecules.

The possible structures/conformations of two PAETA–X chains (9 repeating AETA units) paired with different anions were searched using the Molclus program.[56] Ten initial conformations were obtained, and then xtb software was applied for their optimization, where the conformation with the lowest single point energy was considered as the most stable conformation.[57] The schematic diagrams of the most stable PAETA–X conformations were performed *via* VMD and Multiwfn software,[58,59] as shown in Fig. 4. The typical distance between the two polymer chains of PAETA–Ac (7.91 Å) is significantly larger than that of PAETA–Cl (4.80 Å). Accordingly, the small Cl^- anion (volume of 20.41 Å^3, Table S1, ESI†) with a large charge density can tightly bind the polymer chains together, thereby resulting in a rigid and stiff character of the polymers.[60] The Ac^- anion is larger (61.20 Å^3) and shows a lower charge density, making the polymer chains that are relatively loosely bound with enhanced free volumes and polymer chain mobility, which is conducive to the diffusion of water molecules. Therefore, compared with PAETA–Cl, the higher water sorption capacity of PAETA–Ac is mainly ascribed to the high

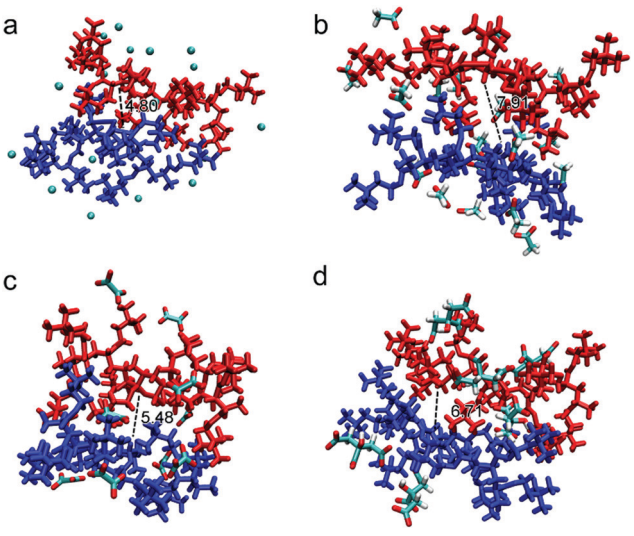

Fig. 4 (a) Simulated structures/conformations of the two PAETA–X polymer chains (9 repeating AETA units) that are bound together with (a) Cl^-, (b) Ac^-, (c) Ox^{2-}, and (d) Cit^{3-}. For clarity, one polymer chain is shown in red and the other in blue.

water affinity of Ac^- anions, and enhanced polymer chain mobility and free volumes.

Compared with the Ac^- anion, the Ox^{2-} and Cit^{3-} anions also contain highly hygroscopic carboxylate groups, but both of them are multi-charged. The typical distances between the two polymer chains of PAETA–Ox and PAETA–Cit are lower than that of PAETA–Ac (Fig. 4), due to the fact that multi-charged Ox^{2-} and Cit^{3-} anions serve as the ionic crosslinkers to bind the polymer chains tightly through strong electrostatic interactions. Thus the polymer chain mobility of PAETA–X hydrogels paired with multi-charged anions is decreased. Therefore, compared with PAETA–Ac, the lower water sorption capacity and lower water affinity of PAETA–Ox and PAETA–Cit are mainly ascribed to the crosslinking effect between the polymer chains and anions.

Water-sorption-driven cooling application

Due to the ongoing global warming and rapid urbanization, the demand of electrical energy by air conditioning systems has increased remarkably over the past decade. Recently, the sorption-driven cooling process has been widely investigated for air-conditioning purposes whose advantages are that water can be used as the working fluid and the low thermal energy sources can be used as the driving energy. The sorption-driven cooling process is based on a sorption–desorption cycle of a working fluid, where useful cold is produced during the evaporation of the working fluid (Fig. S5, ESI†). During the sorption step, the working fluid is evaporated, then sorbed by the sorbent, and heat is taken up from the evaporator (Q_{ev}) leading to a decrease in temperature. When the sorbent becomes saturated, regeneration is then started by using the input of useful heat (Q_{des}) to desorb the working fluid. One can operate such a sorption–desorption cycle as sorption chillers to produce cold at lower temperature by making use of Q_{ev}.[10] More detailed mechanistic discussions and calculations are shown in Supplementary Note S2–4 in the ESI.†

Water-sorption-driven cooling could be used for air-conditioning purposes. The coefficient of performance for cooling (COP_C) is used to describe its energy efficiency, which is defined as the ratio of the useful cooling energy output to the energy input.[10] To calculate the COP_C values, the concept of a characteristic curve was adopted. The characteristic curve combines the pressure and temperature into a single parameter, sorption potential (A), that is related to the Gibbs free energy of sorption. The characteristic curves were first validated by two water sorption isotherms measured at temperatures of 25 °C and 50 °C (Supplementary Note S2 and Eqn S2, ESI†), which almost completely overlapped to form one single characteristic curve (Fig. 5a). This confirms the suitability of the characteristic curves for PAETA–X sorbents. Starting with the characteristic curves, the water vapor sorption isotherms at any other temperatures (30–90 °C) can be extrapolated for PAETA–X sorbents (Fig. S6, ESI†).

For air-conditioning applications, the evaporation temperature (T_{ev}) was set as 10 °C and the condensation temperature (T_{con}) was set as 30 °C (Fig. S7, ESI†) according to the literature

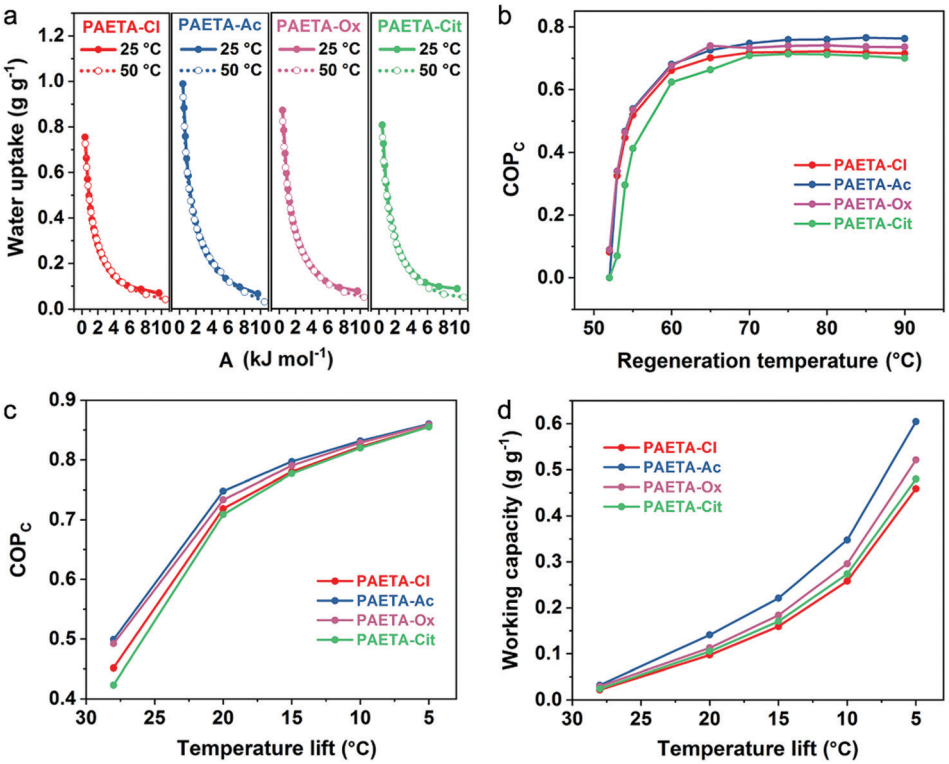

Fig. 5 (a) Characteristic curves of PAETA–X at 25 °C and 50 °C, (b) COP_C as a function of sorbent regeneration temperature for cooling applications (T_{ev} = 10 °C, T_{con} = 30 °C with a temperature lift of 20 °C), (c) COP_C and (d) working capacity (ΔW) as a function of temperature lift for PAETA–X hydrogels at T_{des} of 70 °C (working conditions: T_{ev} = 7 °C, T_{con} = 35 °C with a temperature lift of 28 °C, and T_{con} = 30 °C with the temperature lift of 20–5 °C).

reports,[10,11,13,14] since this working condition was commonly used to evaluate the cooling performance of novel sorbent materials. Based on the water vapor sorption isotherms at different temperatures (30–90 °C), the COP_C values at the different regeneration temperatures were obtained (the calculation process is shown in Supplementary Note S3, S4 and Eqn S3–S8, ESI†). As shown in Fig. 5b, the COP_C value was ~0.66, 0.68, 0.67, and 0.63 at the regeneration temperature of 60 °C, increased to ~0.72, 0.75, 0.73, and 0.71 at the regeneration temperature of 70 °C, and stayed constant thereafter for PAETA–Cl, PAETA–Ac, PAETA–Ox, and PAETA–Cit, respectively. Clearly, PAETA–Ac has the highest COP_C among all due to its highest water working capacity (ΔW, mass difference between the maximal and minimum uptakes of water).

For practical sorption cooling, typical T_{ev} could be 5–10 °C and T_{con} could be 30–45 °C depending on the climate conditions.[61–63] Temperature lift is the difference between T_{con} and T_{ev} and is interpreted as the achievable decrease in temperature for cooling purposes. Different temperature lifts can be used for different working requirements for air-conditioning purposes, and thus the working capacity and COP_C with different temperature lifts were calculated and compared. As shown in Fig. 5c, the COP_C value increased with a decrease in temperature lift because of the increase in working capacity (Fig. 5d). For instance, the working capacity of PAETA–Ac increased from ~0.035 to 0.6 g g^{-1} when the temperature lift was reduced from 28 to 5 °C, leading to the COP_C increasing from ~0.50 to 0.86 at a regeneration temperature of 70 °C.

The stability of PAETA–X hydrogels was studied *via* multiple water vapor sorption–desorption cycles. As shown in Fig. S9 (ESI†), after 10 cycles, no obvious changes in the water uptake were observed for all hydrogels, indicating their stable water sorption and desorption performance. For practical applications, it is important to control the corrosivity of water vapor sorbents, because the corrosion can cause severe metal equipment damage and increase the costs of repairing or replacing the equipment. In Fig. S10 (ESI†), the corrosivity of PAETA–X was examined with aluminum plates after 60 days of intimate contact under ambient conditions (~21 °C, ~60% RH). As can be seen, very visually obvious corrosion occurred to the aluminum plate in contact with the PATEA-Cl hydrogel, due to severe pitting corrosion of Cl^- towards metals.[64] In contrast, the aluminum plates in contact with PAETA–Ac, PAETA–Ox, and PAETA–Cit hydrogels all showed no obvious corrosion, indicating that these halide-free materials are safe and stable even for active metals like aluminum. It should be noted that the test is conducted in the presence of water vapor, which is a more harsh environment than in a dry state. Furthermore, Ac^-, Ox^{2-}, and Cit^{3-} have been reported as corrosion inhibitors since they can form complexes with metals that act as a protective layer on the surface of metals.[65–67] These results indicate that after exchanging Cl^- with Ac^-, Ox^{2-}, and Cit^{3-}, the chloride-free PAETA–X hydrogels can significantly reduce the corrosion damage to metal products, which is a great advantage for this type of water sorbent.

Silica gels are widely studied as the sorbents for sorption-driven cooling applications, but they show relatively low water working capacity that limits the cooling performance.[61–63] Integrating hygroscopic salts (*e.g.*, LiCl) into silica gel can increase the working capacity and lead to high cooling performance, but the leaking and corrosion problems of the salts remain.[14] Aluminophosphates (AlPOs), silica-aluminophosphates (SAPOs), and MOFs have also been developed as sorbents. Unfortunately, the production of these materials usually requires high temperatures and rigorous conditions.[10,63] Since PAETA–X hydrogels have the advantages of reduced corrosiveness, facile fabrication, solid state, and relatively high water working capacity, they show a very promising prospect in air-conditioning applications.

For practical air-conditioning applications, the PAETA–X hydrogel has the potential to be used in sorption beds by coating to the surface of the heat exchanger or integrating into porous silica gel, expanded graphite, metallic foam, and activated carbon fiber to form composite sorbents, which can be achieved through grafting, coating, or composite methods.[45,61–63,68–70]

Atmospheric water harvesting application

A typical AWH test involves water sorption and desorption processes where water vapor sorption occurs at night-time while solar-assisted desorption, condensation, and thus water production occur during the daytime. Carbon nanotubes (CNTs) were introduced into PAETA–Ac hydrogel as the photothermal component.[15] As shown in Fig. 6a, the PAETA–Ac/CNT hydrogel pieces with different shapes can easily adhere together. Indeed, ~20.0 g of PAETA–Ac/CNT hydrogel could steadily attach to the backside of a glass dish unassisted (14.5 × 14.5 cm^2, inset of Fig. 6b), which was used for the outdoor AWH test.

The adhesion performance of a PAETA–Ac/CNT hydrogel to diverse materials was characterized by using lap shear tests,[71,72] where the PAETA–Ac/CNT hydrogel was sandwiched between a pair of glass slides and a pair of stainless steel sheets, respectively. The assemblies were stretched from both ends until separation or fracture. Fig. S11 (ESI†) shows representative adhesion strength–displacement curves for the PAETA–Ac/CNT hydrogel on glass and stainless steel. As can be seen, in the dry state, the adhesion strength of PAETA–Ac/CNT on the glass and stainless steel was 649.5 and 557.3 kPa respectively, which was significantly larger than that in the wet state (16.9 kPa on glass, 12.8 kPa on stainless steel, Fig. S11c and d, ESI†). This is because the hydrogen bond interactions between PAETA–Ac/CNT hydrogel and glass or stainless steel endow high adhesion strengths in the dry state. While, in the wet state, water molecules can interact with various groups of the PAETA–Ac/CNT hydrogel directly, which weakens the interactions between the hydrogel and glass/stainless steel.[72,73] Although PAETA–Ac/CNT in a wet state shows weakened adhesion strength, it can still withstand a load that is 1000 times its own weight (insets of Fig. S11d, ESI†). Due to the good adhesion performance, the PAETA–Ac/CNT hydrogel can adhere to the surface of a glass dish easily for outdoor AWH. The adhesion performance is also beneficial for air-conditioning applications by adhering hydrogels to the surface of a metal heat exchanger.

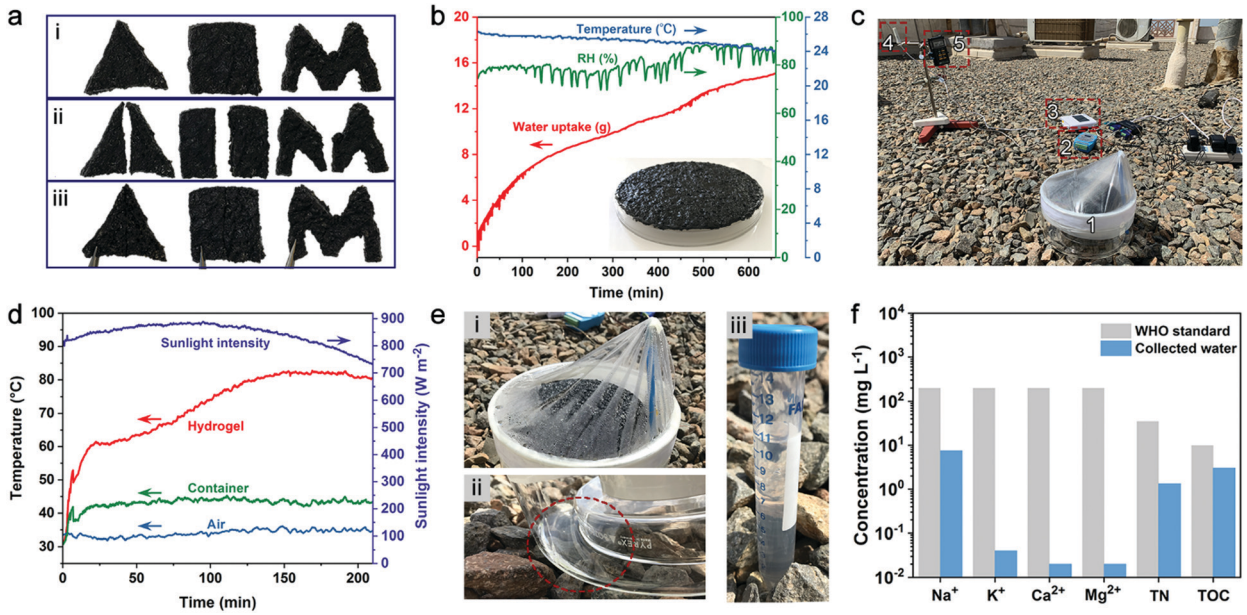

Fig. 6 (a) Tailored PAETA–Ac/CNT hydrogels with triangle, square, and M shapes. The hydrogels (i) before cutting, (ii) after cutting, and (iii) after adhesion together by gentle contact. (b) Water uptake of PAETA–Ac/CNT hydrogel and the ambient conditions in the outdoor water vapor sorption experiment. Inset is a digital photo of the PAETA–Ac/CNT hydrogel attached to the glass dish. (c) Digital photo of the AWH system for the outdoor AWH test with the (1) AWH device, (2) thermocouple temperature transfer module, (3) thermohygrometer, (4) sensor of thermohygrometer, and (5) solar power meter. (d) Sunlight intensity variation and temperature changes of the hydrogel, container, and ambient air in the outdoor AWH experiment (water production step). (e) Digital photos of (i) the AWH device, (ii) condensed water at the bottom of the container, and (iii) collected water at the end of the outdoor water desorption process. (f) The quality of collected water from an outdoor AWH test.

During the outdoor water sorption process, PAETA–Ac/CNT hydrogel was exposed to ambient conditions to sorb water vapor between 7 : 00 pm on April 4, 2020 and 6 : 00 am on April 5, 2020 (KAUST campus, Thuwal, Saudi Arabia), whose weather conditions are shown in Fig. 6b. Then the hydrogel with ~15.1 g of the sorbed water was placed inside an enclosed device with a transparent plastic top wrap, which was then exposed to natural sunlight from 10 : 30 am to 2 : 00 pm on April 5, 2020 (Fig. 6c and Fig. S12, ESI†). Due to the excellent photothermal property of CNTs, the hydrogel layer was heated up to ~60 °C within the first 17 min before reaching a steady-state temperature of ~82 °C by ~150 min (Fig. 6d). At 2 : 00 pm, ~10.7 g water, with a rate of ~0.53 g g^{-1}, was collected by the device (Fig. 6e). The quality of the collected water was analyzed, and the results show that the total organic carbon (TOC), total nitrogen (TN), Na^+, K^+, Ca^{2+}, and Mg^{2+} concentrations of the water were all lower than the WHO standard for drinking water (Fig. 6f).[74]

3. Conclusions

In summary, we have demonstrated the synthesis of PAETA–X hydrogels which are quaternary ammonium-based crosslinking polycations paired with benign-anions. PAETA–X hydrogels with the benign-anions not only provide improved water vapor sorption capacity but also have reduced corrosivity to metal. PAETA–X hydrogels are crosslinked, possess chemical and physical stability, and have solid state when wet. PAETA–X hydrogels are versatile vapor sorbents working in a wide range of relative humidities. PAETA–Ac produces a COP_C of 0.75 with a temperature lift of 20 °C at a low regeneration temperature of 70 °C during an air-conditioning process. PAETA–Ac also produces ~0.53 g g^{-1} fresh water in an outdoor field AWH test from one cycle. The synthesis method of halide-free PAETA–X developed in this work provides a new route for the fabrication of better water vapor sorbents for significant applications at the water-energy nexus.

4. Experimental section

Materials

[2-(Acryloyloxy)ethyl]trimethylammonium chloride solution (AETA-Cl; 80 wt% in water), ammonium persulfate (APS), *N*,*N*′-methylenebisacrylamide (BIS), *N*,*N*,*N*′,*N*′-tetramethylethylenediamine (TEMED), sodium chloride (NaCl), sodium acetate (NaAc), sodium oxalate (Na_2Ox), and sodium citrate dihydrate (Na_3Cit) were purchased from Sigma-Aldrich. Deionized water (18.2 MΩ cm) was used for all experiments. All chemicals were used as received without further purification.

Fabrication of PAETA–X hydrogels

The PAETA–Cl hydrogel was fabricated by free radical polymerization of AETA-Cl monomer, which was initiated by APS in the presence of BIS as the crosslinking agent. Briefly, 2 mg of BIS, and 10 mg of APS were added into 2 mL of 50 wt% AETA-Cl aqueous solution. Then, the mixed solution was treated by ultrasonication in an ice–water bath for 5 min and then treated with nitrogen for 10 min to remove the oxygen in the solution.

Finally, 10 μL of TEMED was added, and then the mixed solution was sealed and kept at room temperature for 12 h to polymerize into the original PAETA–Cl hydrogel.

The purified PAETA–Cl hydrogel and PAETA–X hydrogels paired with other counter anions (Ac^-, Ox^{2-} and Cit^{3-}) were prepared *via* the ion-exchange method. Briefly, the original PAETA–Cl hydrogel was immersed in an aqueous solution of 5 wt% NaCl, 5 wt% NaAc, 3 wt% Na_2Ox, and 5 wt% Na_3Cit for 12 h 3 times followed by immersion in water for 12 h 6 times, respectively. The hydrogel was finally dried at 80 °C in an oven to obtain purified PAETA–X, with X being Cl^-, Ac^-, Ox^{2-} or Cit^{3-}.

Material characterization

ATR-FTIR spectra of PAETA–X were obtained on a Nicolet iS10 FTIR spectrometer by using the Thermo Scientific Smart iTX ATR sampling accessory. Energy dispersive spectroscopy (EDS) spectra were performed using an EDAX EDS detector attached to an FEI Quanta 600 SEM. PAETA–X hydrogels were placed in contact with aluminum plates for 60 days to assess their corrosivity by an optical microscope (Nikon AZ100M). The thermal stability of the hydrogels was determined by a thermogravimetric analyzer (TGA, NETZSCH TG 209 *F1 Iris*®) with the heating rate of 10 °C min^{-1} under a nitrogen atmosphere. The glass transition temperature (T_g) and specific heat capacity (c_p) of PAETA–X were determined using a differential scanning calorimeter (DSC, TA Discovery DSC 250) under the modulation mode with the temperature range from −80 to 120 °C at a heating rate of 2 °C min^{-1} in a nitrogen atmosphere. Water vapor sorption/desorption isotherms were measured by an intelligent gravimetric analyzer (IGA, Hiden Isochema IGAsorp-CT). Static water vapor sorption–desorption curves and multiple cycles of water sorption–desorption were performed on a simultaneous thermal analyzer (STA, NETZSCH STA 449 *F3 Jupiter*®) connected with a modular humidity generator (ProUmid GmbH & Co. KG, MHG32). The humidity was controlled by a humidified nitrogen gas flow, which was passed through the thermogravimetric balance. It is worth mentioning that the water vapor was produced at room temperature (~21 °C), which was lower than the temperature of thermogravimetric balance in our tests. The adhesion performance of PAETA–Ac/CNT hydrogel was determined through lap shear tests using a Universal Testing Machine (Instron 5944). A hydrogel (20 × 26 × 1 mm^3) was sandwiched between two glass slides or two stainless steel sheets. All tests were performed at a tensile speed of 60 mm min^{-1} at room temperature.

In conducting the outdoor AWH experiment, a simple and homemade all-in-one device was used. For the outdoor test, 2.5 wt‰ CNT[15] (mass ratio of CNT and AETA-Cl monomer) was added in the synthesis process of PAETA–Cl, and PAETA–Ac/CNT hydrogel was obtained following otherwise the same procedure. A thermocouple temperature transfer module (SULINKIOT RS20K-C) with two 0.5 mm K-type thermocouple sensors was used to monitor the temperature changes of the hydrogel and condenser. A thermohygrometer (SULINKIOT CX03) was used to record the RH and temperature of ambient air, and a solar power meter (TES-1333R) was used to record the sunlight intensity. The ion concentrations of the collected water were detected using the inductively coupled plasma-optical emission spectrometry instrument (ICP-OES, Agilent 5110). The total organic carbon (TOC) and total nitrogen (TN) were detected using a total organic carbon analyzer (TOC-L, SHIMADZU).

Conflicts of interest

There are no conflicts to declare.

Acknowledgements

This work was supported by King Abdullah University of Science and Technology (KAUST). The authors are grateful to KAUST for very generous financial support. We appreciate Dr Jingyu Liu at the ACL of KAUST for the support of DSC tests. We appreciate Yangyang Xin and Prof. Gilles Lubineau at the COHMAS Laboratory, Physical Sciences and Engineering Division (PSE) of KAUST for the help and support with adhesion performance tests.

References

1 Y. Guo, J. Bae, Z. Fang, P. Li, F. Zhao and G. Yu, *Chem. Rev.*, 2020, **120**, 7642–7707.
2 C. Chen, Y. Kuang, S. Zhu, I. Burgert, T. Keplinger, A. Gong, T. Li, L. Berglund, S. J. Eichhorn and L. Hu, *Nat. Rev. Mater.*, 2020, **5**, 642–666.
3 F. Zhu, L. Wang, B. Demir, M. An, Z. L. Wu, J. Yin, R. Xiao, Q. Zheng and J. Qian, *Mater. Horiz.*, 2020, **7**, 3187–3195.
4 P. Wang, *Environ. Sci.: Nano*, 2018, **5**, 1078–1089.
5 Y. Tu, R. Wang, Y. Zhang and J. Wang, *Joule*, 2018, **2**, 1452–1475.
6 C. Zhang, H.-Q. Liang, Z.-K. Xu and Z. Wang, *Adv. Sci.*, 2019, **6**, 1900883.
7 W. Wang, Y. Shi, C. Zhang, S. Hong, L. Shi, J. Chang, R. Li, Y. Jin, C. Ong, S. Zhuo and P. Wang, *Nat. Commun.*, 2019, **10**, 3012.
8 X. Zhao, L.-M. Peng, C.-Y. Tang, J.-H. Pu, X.-J. Zha, K. Ke, R.-Y. Bao, M.-B. Yang and W. Yang, *Mater. Horiz.*, 2020, **7**, 855–865.
9 R. Li, Y. Shi, M. Wu, S. Hong and P. Wang, *Nat. Sustainable*, 2020, **3**, 636–643.
10 M. F. de Lange, K. J. F. M. Verouden, T. J. H. Vlugt, J. Gascon and F. Kapteijn, *Chem. Rev.*, 2015, **115**, 12205–12250.
11 S. Wang, J. S. Lee, M. Wahiduzzaman, J. Park, M. Muschi, C. Martineau-Corcos, A. Tissot, K. H. Cho, J. Marrot, W. Shepard, G. Maurin, J.-S. Chang and C. Serre, *Nat. Energy*, 2018, **3**, 985–993.
12 K. H. Cho, D. D. Borges, U. H. Lee, J. S. Lee, J. W. Yoon, S. J. Cho, J. Park, W. Lombardo, D. Moon, A. Sapienza, G. Maurin and J.-S. Chang, *Nat. Commun.*, 2020, **11**, 5112.
13 L. Garzón-Tovar, J. Pérez-Carvajal, I. Imaz and D. Maspoch, *Adv. Funct. Mater.*, 2017, **27**, 1606424.
14 K. Yang, Y. Shi, M. Wu, W. Wang, Y. Jin, R. Li, M. W. Shahzad, K. C. Ng and P. Wang, *J. Mater. Chem. A*, 2020, **8**, 1887–1895.
15 R. Li, Y. Shi, M. Alsaedi, M. Wu, L. Shi and P. Wang, *Environ. Sci. Technol.*, 2018, **52**, 11367–11377.
16 R. Li, Y. Shi, M. Wu, S. Hong and P. Wang, *Nano Energy*, 2020, **67**, 104255.

17 J. Xu, T. Li, J. Chao, S. Wu, T. Yan, W. Li, B. Cao and R. Wang, *Angew. Chem., Int. Ed.*, 2020, **59**, 5202–5210.
18 G. Yilmaz, F. L. Meng, W. Lu, J. Abed, C. K. N. Peh, M. Gao, E. H. Sargent and G. W. Ho, *Sci. Adv.*, 2020, **6**, eabc8605.
19 X. Wang, X. Li, G. Liu, J. Li, X. Hu, N. Xu, W. Zhao, B. Zhu and J. Zhu, *Angew. Chem., Int. Ed.*, 2019, **58**, 12054–12058.
20 F. Zhao, X. Zhou, Y. Liu, Y. Shi, Y. Dai and G. Yu, *Adv. Mater.*, 2019, **31**, 1806446.
21 H. Yao, P. Zhang, Y. Huang, H. Cheng, C. Li and L. Qu, *Adv. Mater.*, 2020, **32**, 1905875.
22 Y. Byun and A. Coskun, *Angew. Chem., Int. Ed.*, 2018, **57**, 3173–3177.
23 F. Ni, N. Qiu, P. Xiao, C. Zhang, Y. Jian, Y. Liang, W. Xie, L. Yan and T. Chen, *Angew. Chem., Int. Ed.*, 2020, **59**, 19237–19246.
24 H. Qi, T. Wei, W. Zhao, B. Zhu, G. Liu, P. Wang, Z. Lin, X. Wang, X. Li, X. Zhang and J. Zhu, *Adv. Mater.*, 2019, **31**, 1903378.
25 D. K. Nandakumar, Y. Zhang, S. K. Ravi, N. Guo, C. Zhang and S. C. Tan, *Adv. Mater.*, 2019, **31**, 1806730.
26 A. LaPotin, Y. Zhong, L. Zhang, L. Zhao, A. Leroy, H. Kim, S. R. Rao and E. N. Wang, *Joule*, 2021, **5**, 166–182.
27 N. Hanikel, M. S. Prévot and O. M. Yaghi, *Nat. Nanotechnol.*, 2020, **15**, 348–355.
28 H. Kim, S. R. Rao, E. A. Kapustin, L. Zhao, S. Yang, O. M. Yaghi and E. N. Wang, *Nat. Commun.*, 2018, **9**, 1191.
29 C. Olkis, H. Dong, S. Brandani and G. Santori, *Environ. Sci. Technol.*, 2020, **54**, 3591–3598.
30 B. Li, L. Hua, Y. Tu and R. Wang, *Joule*, 2019, **3**, 1427–1436.
31 Y. Zhang, L. Wu, X. Wang, J. Yu and B. Ding, *Nat. Commun.*, 2020, **11**, 3302.
32 B. Xiang, P. K. Patra, S. A. Montzka, S. M. Miller, J. W. Elkins, F. L. Moore, E. L. Atlas, B. R. Miller, R. F. Weiss, R. G. Prinn and S. C. Wofsy, *Proc. Natl. Acad. Sci. U. S. A.*, 2014, **111**, 17379.
33 B. Chen, X. Zhao and Y. Yang, *ACS Appl. Mater. Interfaces*, 2019, **11**, 15616–15622.
34 A. Entezari, M. Ejeian and R. Wang, *ACS Mater. Lett.*, 2020, **2**, 471–477.
35 S. Pu, J. Fu, Y. Liao, L. Ge, Y. Zhou, S. Zhang, S. Zhao, X. Liu, X. Hu, K. Liu and J. Chen, *Adv. Mater.*, 2020, **32**, 1907307.
36 T. Brünig, M. Maurer and R. Pietschnig, *ACS Sustainable Chem. Eng.*, 2017, **5**, 7228–7239.
37 D. Kundu, E. Talaie, V. Duffort and L. F. Nazar, *Angew. Chem., Int. Ed.*, 2015, **54**, 3431–3448.
38 H. M. L. Thijs, C. R. Becer, C. Guerrero-Sanchez, D. Fournier, R. Hoogenboom and U. S. Schubert, *J. Mater. Chem.*, 2007, **17**, 4864–4871.
39 J. Byun, H. A. Patel, D. Thirion and C. T. Yavuz, *Polymer*, 2017, **126**, 308–313.
40 R. Mohanrao and K. M. Sureshan, *Angew. Chem., Int. Ed.*, 2018, **57**, 12435–12439.
41 K. Matsumoto, N. Sakikawa and T. Miyata, *Nat. Commun.*, 2018, **9**, 2315.
42 H. Mittal, A. A. Alili and S. M. Alhassan, *Colloids Surf., A*, 2020, **599**, 124813.
43 X. Zhou, P. Zhang, F. Zhao and G. Yu, *ACS Mater. Lett.*, 2020, 1419–1422, DOI: 10.1021/acsmaterialslett.0c00439.
44 F. Ni, P. Xiao, N. Qiu, C. Zhang, Y. Liang, J. Gu, J. Xia, Z. Zeng, L. Wang, Q. Xue and T. Chen, *Nano Energy*, 2020, **68**, 104311.
45 K. Yang, T. Pan, I. Pinnau, Z. Shi and Y. Han, *Nano Energy*, 2020, **78**, 105326.
46 Y. Chen, X. Sun, C. Yan, Y. Cao and T. Mu, *J. Phys. Chem. B*, 2014, **118**, 11523–11536.
47 S. L. Banerjee and N. K. Singha, *Soft Matter*, 2017, **13**, 9024–9035.
48 F. Li, L. Koopal and W. Tan, *Sci. Rep.*, 2018, **8**, 2060.
49 J.-W. Park and J. S. Shumaker-Parry, *J. Am. Chem. Soc.*, 2014, **136**, 1907–1921.
50 M. Isik, R. Gracia, L. C. Kollnus, L. C. Tomé, I. M. Marrucho and D. Mecerreyes, *ACS Macro Lett.*, 2013, **2**, 975–979.
51 P. Naert, K. Rabaey and C. V. Stevens, *Green Chem.*, 2018, **20**, 4277–4286.
52 G. Szakonyi and R. Zelkó, *Int. J. Pharm. Invest.*, 2012, **2**, 18–25.
53 Y. Cao, Y. Chen, X. Sun, Z. Zhang and T. Mu, *Phys. Chem. Chem. Phys.*, 2012, **14**, 12252–12262.
54 A. J. Rieth, S. Yang, E. N. Wang and M. Dincă, *ACS Cent. Sci.*, 2017, **3**, 668–672.
55 Q. Shao and S. Jiang, *J. Phys. Chem. B*, 2014, **118**, 7630–7637.
56 T. Lu, *Molclus program, Version 1.9*, Beijing Kein Research Center for Natural Science, China, 2021http://www.keinsci.com/research/molclus.html.
57 C. Bannwarth, E. Caldeweyher, S. Ehlert, A. Hansen, P. Pracht, J. Seibert, S. Spicher and S. Grimme, *Wiley Interdiscip. Rev.: Comput. Mol. Sci.*, 2020, e01493.
58 W. Humphrey, A. Dalke and K. Schulten, *J. Mol. Graphics*, 1996, **14**, 33–38.
59 T. Lu and F. Chen, *J. Comput. Chem.*, 2012, **33**, 580–592.
60 P. Guo, H. Zhang, X. Liu and J. Sun, *ACS Appl. Mater. Interfaces*, 2018, **10**, 2105–2113.
61 Y. Liu, R. Wang and Z. Xia, *Appl. Therm. Eng.*, 2005, **25**, 359–375.
62 H. T. Chua, K. C. Ng, A. Malek, T. Kashiwagi, A. Akisawa and B. B. Saha, *Int. J. Refrig.*, 1999, **22**, 194–204.
63 S. K. Henninger, F. Jeremias, H. Kummer, P. Schossig and H.-M. Henning, *Energy Procedia*, 2012, **30**, 279–288.
64 G. S. Frankel, J. D. Vienna, J. Lian, J. R. Scully, S. Gin, J. V. Ryan, J. Wang, S. H. Kim, W. Windl and J. Du, *npj Mater. Degrad.*, 2018, **2**, 15.
65 G. Kılınççeker and C. Menekşe, *Prot. Met. Phys. Chem. Surf.*, 2015, **51**, 659–666.
66 W. Zhang, H.-J. Li, L. Chen, J. Sun, X. Ma, Y. Li, C. Liu, X. Han, B. Pang and Y.-C. Wu, *Desalination*, 2020, **486**, 114482.
67 H. Jeziorowski and B. Moser, *Chem. Phys. Lett.*, 1985, **120**, 41.
68 A. Entezari, M. Ejeian and R. Wang, *Appl. Therm. Eng.*, 2019, **161**, 114109.
69 I. Hideo, K. Fujio, H. Akihiko, H. Naoto and M. Akito, *Therm. Sci. Eng.*, 2008, **15**, 141–150.
70 R. P. Singh, V. K. Mishra and R. K. Das, *IOP Conf. Ser.: Mater. Sci. Eng.*, 2018, **404**, 012005.
71 X. Pei, H. Zhang, Y. Zhou, L. Zhou and J. Fu, *Mater. Horiz.*, 2020, **7**, 1872–1882.
72 M. Shan, C. Gong, B. Li and G. Wu, *Polym. Chem.*, 2017, **8**, 2997–3005.
73 C. White, K. T. Tan, D. Hunston, K. Steffens, D. L. Stanley, S. K. Satija, B. Akgun and B. D. Vogt, *Soft Matter*, 2015, **11**, 3994–4001.
74 *Guidelines for Drinking-Water Quality*, WHO Press, 4th edn, 2011.